Mineralogy and Petrology (1994) 50: 173–193

Mineralogy and Petrology

Pb–Nd–Sr Isotopic and Geochemical Constraints on the Origin of the 1.54–1.56 Ga Salmi Rapakivi Granite—Anorthosite Batholith (Karelia, Russia)

L. A. Neymark, Yu. V. Amelin, and A. M. Larin

Institute of Precambrian Geology and Geochronology, Russian Academy of Science, St. Petersburg, Russia

With 7 Figures

Received October 14, 1991;
accepted October 30, 1992

Summary

The Salmi batholith is situated on the eastern edge of the EW-trending anorthosite-rapakivi granite belt of the Fennoscandian shield, at the contact between Proterozoic and Archean crustal domains. The tectonic setting and high K, Rb, Nb, Y, Zr, REE (except Eu), F, Sn, Be, and Li contents of the Salmi batholith indicate that it represents typical subalkaline A-type and within plate granites. Gabbro-anorthosites of the batholith demonstrate a concordant U–Pb apatite age of 1563 ± 9 (2σ) Ma and a Sm–Nd internal isochron age of 1552 ± 69 Ma. Zircons from amphibole-biotite granites have an upper concordia intercept U–Pb age of 1543 ± 8 Ma. An older inherited zircon component with elevated Th/U ratio is found in zircons separated from K-feldspar ovoids. Rb-Sr internal errorchron for the granites yields an age of 1455 ± 17 Ma, probably the time of completion of postmagmatic processes within the batholith. The gabbro-anorthosites and granites show similar initial Nd, Sr, and feldspar Pb isotope compositions ($\varepsilon_{Nd} = -6.5$ to -8.2; $\mu_2 = 8.6$ to 8.9; $\kappa_2 = 3.9$ to 4.0; $I_{Sr} = 0.7052$ to 0.7057 for the basic rocks, and $\varepsilon_{Nd} = -6.2$ to -8.9; $\mu_2 = 8.1$ to 9.2; $\kappa_2 = 4.0$ to 4.4; $I_{Sr} = 0.7050$ to 0.7072 for the granites). Two-stage neodymium T_{DM} model ages for both assemblages range from 2.60 to 2.80 Ga. Old LREE-enriched sources with low time-integrated U/Pb and Rb/Sr and elevated Th/U ratios were involved in the formation of both the gabbro-anorthosites and the granites. Bulk contamination with crustal materials cannot explain the data for the basic rocks. Selective incorporation of Pb, Sr, and Nd from Archean lower crust is needed, or else, the gabbro-anorthosites may have been derived from an isotopically anomalous subcontinental mantle source. The ascent of a mantle diapir resulted in anatexis of the lower crust and formation of the parent magma for the rapakivi granites.

Zusammenfassung

Pb–Nd–Sr Isotope, und geochemische Daten: Bedeutung für die Entstehung des 1,54–1,56 Salmi Rapakivi Granit-Anorthosit-Batholithen (Karelia, Rußland).

Der Salmi-Batholith ist am östlichen Rand des Ost-West streichenden Anorthosit-Rapakivi-Granitgürtels des fennoskandischen Schildes am Kontakt zwischen proterozoischen und archaischen Krustenbereichen gelegen. Die tektonische Position und hohe K, Rb, Nb, Y, Zr, REE (mit Ausnahme von Eu), F, Sn, Be und Li-Gehalte des Salmi-Batholithen weisen darauf hin, daß es sich hier um einen typischen subalkalischen A-Typ und "within plate" Granit handelt. Gabbro-Anorthosite des Batholithen zeigen ein konkordantes U–Pb Apatit alter von 1563 ± 9 (2σ) Ma und ein internes Sm-Nd Isochronenalter von 1552 ± 69 Ma. Zirkone aus den Amphibolit-Biotitgraniten haben ein oberes Concordia U-Pb Alter von 1543 ± 8Ma. Ein ältere, ererbte Zirkonkomponente mit erhöhtem Th/U Verhältnis kommt in Zirkonen, die von K-Feldspat Ovoiden abgetrennt wurden, vor. Eine interne Rb–Sr Errorchrone für die Granite ergibt ein Alter von 1455 ± 7 Ma. Dies repräsentiert wahrscheinlich die Zeit des Abschlusses postmagmatischer Prozesse innerhalb des Batholithen. Die Gabbro-Anorthosite und Granite zeigen ähnliche Nd, Sr und Feldspat Pb Isotopenzusammensetzungen (ε_{Nd} = −6.5 to 8.2; μ_2 = 8.6 to 8.9; K_2 = 3.9 to 4.0; I_{Sr} = 0.7052 to 0.7057 für die mafischen Gesteine, und ε_{Nd} = −6.2 to −8.9; μ_2 = 8.1 to 9.2; K_2 = 4.0 to 4.4; I_{Sr} = 0.7050 to 0.7072 für die Granite). Zweistufige Neodymium T_{DM} Modellalter für beide Assoziationen liegen zwischen 2.60 und 2.80 Ga. Alte LREE-angereicherte Quellen mit niedrigen, zeitintegrierten U/Pb und Rb/Sr und erhöhten Th/U Verhältnissen waren bei der Bildung der Gabbro-Anorthosite und Granite involviert. Kontamination mit Krustenmaterial kann die Daten für die basischen Gesteine nicht erklären. Entwederist dazu eine selektive Inkorporation von Pb, Sr und Nd aus der tieferen archaischen Kruste erforderlich oder man muß annehmen, daß die Gabbro-Anorthosite von einer isotopisch anomalen subkontinentalen Mantelquelle stammen. Der Aufstieg eines Mantel-Diapirs führt zu Anatexis der tieferen Kruste und zur Bildung der Ausgangsmagmen für die Rapakivi Granite.

Introduction

Anorthosite-rapakivi granite complexes typically comprise elongated non-continuous belts in Precambrian shield areas and have been formed mainly between 1.75 and 1.0 Ga. Emplacement of these plutons is attributed by most authors to incipient rifting (e.g., *Emslie*, 1985; *Anderson*, 1983; *Windley*, 1983; *Nurmi* and *Haapala*, 1986). *Anderson* (1983) relates these rocks to incipient rift evolution interrupted at an early pre-rift stage, while *Windley* (1983) classifies the intrusion belts as "abortive rift structures". Temporally associated with the anorthosite-rapakivi plutons are bimodal volcanic suites, with a predominance of acidic volcanics as well as quartz porphyry and dolerite dykes.

Within the East European platform the plutons of the anorthosite-rapakivi granite assemblage constitute a NW-trending belt that follows the western margin of the platform and extends for more than 2000 km from Ukraine through Byelorussia, Poland, and the Baltic region to Fennoscandia (Fig. 1). Another ca. 1000 km long EW-trending belt occurs along the southern margin of the Fennoscandian (Baltic) shield. The two belts join in southern Fennoscandia (Fig. 1). The age of the intrusions ranges from 1.77 to 1.54 Ga. The oldest (1.77 to 1.75 Ga) plutons,

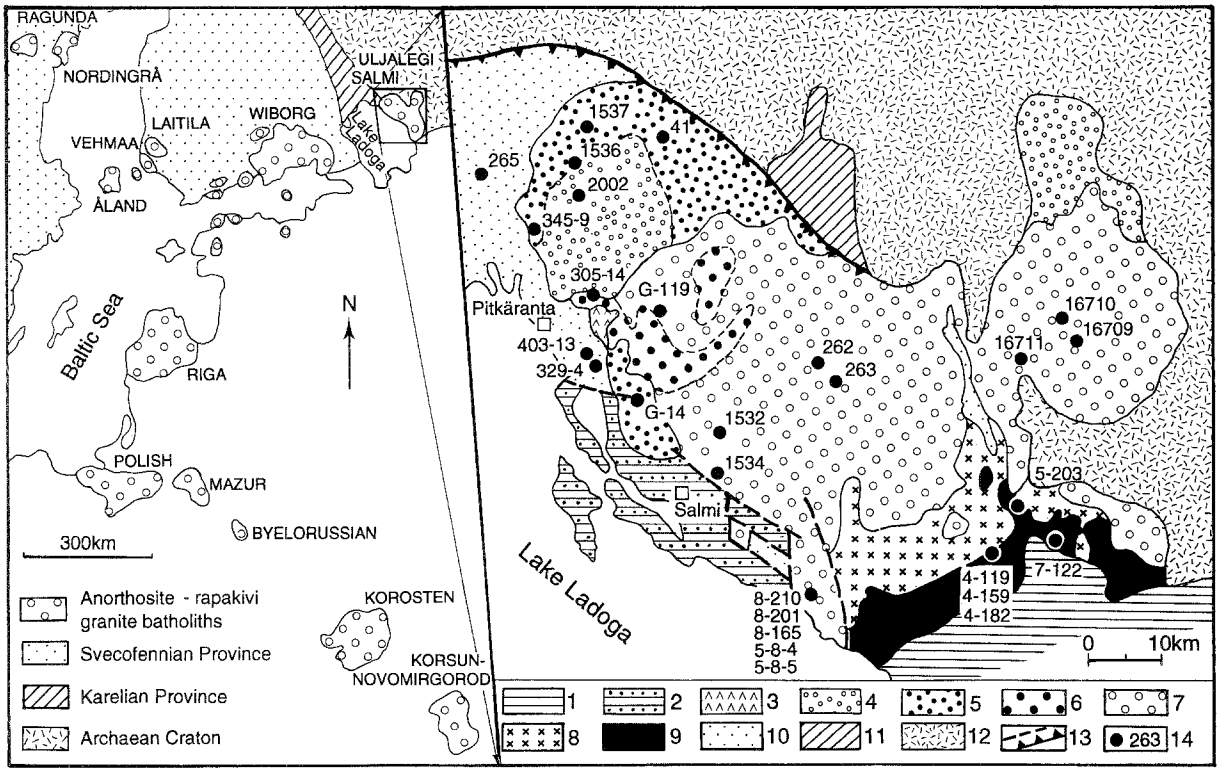

Fig. 1. Lithology of the Salmi anorthosite-rapakivi granite batholith. *1* sedimentary rocks of the East European platform; *2* volcanogenic-terrigenous Jotnian rocks (Salmi suite); *3–9* igneous rocks of the Salmi batholith: *3* albite-lithian siderophyllite granites, *4* porphyritic biotite granites with a fine-grained groudmass, *5* even-grained biotite granite, *6* porphyritic amphibole-biotite granites with a fine-grained groundmass, *7* coarse-grained amphibole-biotite granites (wiborgites and pyterlites), *8* monzonites, *9* gabbronorites, gabbros, anorthosites; *10* Svecokarelian gneiss-schist complex; *11* Jatulian carbonate-terrigenous complex; *12* Lopian (Archean) granite-greenstone complex; *13* thrusts and fractures; *14* sample localities. Plutons of the anorthosite-rapakivi granite assemblage in the East European platform and Fennoscandia are shown in left (modified from *Velikoslavinskiy* et al., 1978)

Korosten and Korsun-Novomirgorod, are found in the Ukrainian shield (*Scherbak* et al., 1989; *J. V. Amelin*, unpublished data), while intrusions defining two age groups are found in the Fennoscandian shield: the 1.65 to 1.62 Ga Wiborg batholith (*Vaasjoki* et al., 1991) and the Laitila, Vehmaa, Åland, and Salmi batholiths with ages between 1.59 and 1.54 Ga (*Vaasjoki*, 1977; *Suominen*, 1991; this study).

There are different opinions about the petrogenesis of the rapakivi granites. The main problems are their geotectonic framework, the source of the magmas, and the genetic relations between rapakivi granites and the associated basic rocks. Geochemical and isotopic data indicate that most of the mainly middle Proterozoic rapakivi-type granites of southeastern Fennoscandia and North America represent reworked early Proterozoic crust (*Rämö* and *Haapala*, 1991; *Emslie*, 1985). The objective of this paper is to evaluate the source nature and to constrain models for the formation of the Salmi batholith and its satellite intrusion Uljalegi (Sotjärvi) which are also associated with Archean crust.

Geological Setting and Internal Structure of the Salmi Batholith

The Salmi batholith cuts late Archean granitoids and supracrustal rocks (greenstone belts) of the Karelian craton, as well as lower Proterozoic metamorphic formations (Jatulian carbonate-terrigenous rocks and Svecokarelian gneisses and schists) (Fig. 1). The batholith was emplaced along an upthrust zone between the Archean and Proterozoic domains. The southwestern part of the batholith is overlain by the middle Proterozoic terrigenous-volcanic Jotnian unit (the Salmi suite) and is intersected by dykes and minor layered intrusions comagmatic with the volcanics of the Salmi suite (Fig. 1).

There are five main rock types in the Salmi batholith: (1) gabbros, gabbronorites, and anorthosites, (2) monzonites and quartz syenites, (3) amphibole-biotite granites, (4) biotite granites, and (5) albite-lithian siderophyllite granites (e.g., *Velikoslavinsky* et al., 1978). The batholith is asymmetrically zoned (Fig. 1). From the southeast, where on the basis of geophysical data a root channel is expected to occur, a regular compositional change is encountered towards northwest. The rocks of the first four

Table 1. *Modal compositions of different rock types within the Salmi batholith*

Mineral*	Anorthosites, gabbros, gabbronorites	Monzonites, syenites	Amphibole-biotite granites	Biotite granites	Albite-Li-siderophyllite granites
Orthopyroxene	1.5 – 29	0.5 – 8.0			
Clinopyroxene	2.0 – 30	8.0 – 17	<1.0		
Olivine	<1.0 – 5.0	<1.0 – 1.5	<1.0	<1.0	
Hornblende	<1.0 – 1.5	1.0 – 4.0			
Hastingsite			0.4 – 1.2		
Biotite	≤1.0	1.0 – 2.0	2.3 – 3.0	2.3 – 2.9	
Li-siderophyllite					2.0 – 4.5
Plagioclase:					
An_{42-54}	48 – 88				
An_{32-50}		31 – 49			
An_{18-28}			8.5 – 12		
An_{05-20}				8.5 – 10.5	
An_{03-10}					40 – 50
Alkali feldspar	<1.0 – 7.0	3.0 – 31	55 – 56.5	51 – 52.5	15 – 20
Quartz	<1.0 – 3.0	5.0 – 20	29 – 33	34.5 – 38	34 – 36
Topaz					0.5 – 1.5
Ilmenite, Titanomagnetite	<1.0 – 15	<1.0 – 6.0	++++	+++	++
Magnetite			+	+++	+
Hematite			+++	+++	+++
Apatite	++++	+++	++	+	+
Fluorite			+++	++++	++++
Zircon	++	++	+++	+++	++
Allanite, bastnaesite			++++	+++	+
Pyrite	+++	+++	+	+	+
Molybdenite			++	+	+
Titanite	+++	++	+	+	+
Cassiterite			+	+	+
Tantalite					++
Xenotime				+	+
Garnet	+	+	+	+	+
Sillimanite			+	+	
Tourmaline			+	+	

*Abundances of major minerals in %, for accessory minerals relative abundances are denoted

groups presumably comprise sheet-like bodies plunging to the southeast. The modal compositions of the rocks are shown in Table 1.

Basic rocks are widespread in the buried southeastern part of the batholith and have been discovered by drilling. They comprise anorthosites, gabbro-anorthosites, gabbros, and gabbronorites, and sometimes show a vertical mutual transition in this order. Monzonites and quartz syenites show a close association with anorthosites and gabbros. These can often be traced along the boundaries between rapakivi granites and gabbronorites. Quartz syenites also occur in the southern part of the Uljalegi intrusion.

Amphibole-biotite rapakivi granites make up two-thirds of the exposed part of the batholith and include four varieties: (1) coarse-grained, often rapakivi-textured amphibole-biotite granites, (2) porphyritic amphibole-biotite granites with a fine-grained groundmass, (3) non-ovoidal coarse-grained amphibole-biotite granites occurring in the central and southern parts of the Uljalegi intrusion, and (4) fine-grained dykes of aplitic granite. The contacts of the amphibole-biotite granites against the wall rocks are usually sharp and have 10 to 50 cm thick chilled margins consisting of fine-grained granite similar in composition to the dyke granites. Non-ovoidal biotite granites cut the amphibole-biotite granites and make up the northern and northwestern parts of the Salmi batholith and the northern part of the Uljalegi intrusion (Fig. 1). Several textural varieties can be distinguished: (1) even-grained granites, (2) porphyritic granites with a fine-grained groundmass, and (3) fine-grained dykes which fill cracks in granites of the first two varieties. The albite-lithian siderophyllite granites are topaz-bearing and comprise several small dykes, stocks, and minor dome-shaped intrusions within the amphibole-biotite granites, biotite granites, and metamorphic country rocks. They usually have a fine-grained aplitic texture, while stockscheider-type pegmatites are often present along the borders and in the apical parts of the dykes and dome structures. The granites of this group show sharp, occasionally bracciated contacts to the surrounding rocks. For a more detailed petrographic description of the Salmi batholith, see *Amelin* et al. (1991).

Analytical Techniques

Isotopic analyses of zircons followed the method described by *Krogh* (1973). The total Pb blank was 0.2 to 1 ng. In some cases, air-abrasion was used applying the *Krogh* (1982) technique, modified by coating the abrasive walls with epoxy impregnated diamond powder for more effective abrasion. The computational algorithm by *Ludwig* (1987) was used for uncertainties and correlations of U/Pb ratios and the ISOPLOT program (*Ludwig*, 1988) was used to calculate discordia and isochrons. Ages were determined using the decay constants of *Steiger* and *Jäger* (1977). All errors are given at the $\pm 2\sigma$ level. Correction for common Pb was made using the Pb isotopic composition of co-existing feldspar leached with HNO_3 (see below).

Pb was separated from apatites and feldspars utilizing the HBr techniques of *Mahnes* et al. (1978). Samples were pretreated either with ETDA sodium salt (apatites) or diluted HNO_3 (feldspars) to remove surface contamination. Powdered feldspars were additionally leached with hot 12N HNO_3 for 5 to 6 hours to remove radiogenic Pb. The total Pb blank was 0.5 to 3.5 ng for apatites and 5 ± 2 ng for the common Pb procedures. Isotopic analysis of Pb was carried out with the aid of

silicagel emitter. Mass-discrimination of 0.0013 ± 0.0003 per amu, determined by numerous measurements of SRM-982, was used to correct for fractionation in the samples. Average ratios for SRM-982 measured during the course of these analyses were $^{206}Pb/^{204}Pb = 36.643$, $^{207}Pb/^{204}Pb = 17.092$, and $^{208}Pb/^{204}Pb = 36.551$. External 2σ error of 0.05% per amu was accepted for real samples.

Rock powders and mineral fractions for Sm–Nd and Rb–Sr studies were dissolved in a $HF + HNO_3$ mixture. Before decomposition, all samples were totally spiked with ^{149}Sm–^{146}Nd and ^{85}Rb–^{84}Sr mixed solutions. Sm and Nd were separated using a two-step procedure: first conventional cation-exchange chromatography and then extraction chromatography on HDEHP-covered teflon powder (*Richard* et al., 1976). Total blanks during the course of this study ranged from 0.03 to 0.2 ng for Sm and from 0.1 to 0.5 ng for Nd. The results were normalized to $^{148}Nd/^{144}Nd = 0.24157$. The mean values for 13 runs of BCR-1 were 6.54 ppm Sm, 28.5 ppm Nd, $^{147}Sm/^{144}Nd = 0.1380$, and $^{143}Nd/^{144}Nd = 0.512633 \pm 0.000005$. Rb and Sr were separated using conventional cation-exhange techniques. Procedure blanks were 0.03 to 0.07 ng for Rb and 0.5 to 0.8 ng for Sr. Sr isotopic ratios were normalized to $^{86}Sr/^{88}Sr = 0.1194$. The mean of four runs of BCR-1 were 45.9 ppm Rb, 329 ppm Sr, $^{87}Rb/^{86}Sr = 0.4027$, and $^{87}Sr/^{86}Sr = 0.705013 \pm 0.000006$. Isotopic measurements were performed on a MAT 261 8-collector mass-spectrometer in static mode.

Geochemistry

Major and trace element data for selected isotopically studied samples are given in Table 2. Geochemically, the Salmi batholith consists of a gabbronorite-anorthosite-monzonite series and a rapakivi granite series. A special feature of the basic rocks are the very low contents of Cr, Ni, Co, V, and Mn and high concentrations of incompatible elements (Table 2 and unpublished data of the authors) as compared with basic rocks of the Proterozoic anorthosite complexes in general. In comparison with the Finnish gabbro-anorthosites (*Rämö*, 1991), they are richer in Ba, Pb, Th, Nb, Y, Zr, Ti, F, and REE and poorer in K_2O, Rb, and Sr. The gabbronorite 4–182 (Table 2) shows Nd and Sm abundances approaching those of the rapakivi granites of the major intrusive phase of the batholith and also shows abnormally high contents of Zr (901 ppm) and Ba (4610 ppm). $(La/Yb)_N$ and $(Eu/Eu^*)_N$ ratios in the basic rocks range from 8.24 to 9.05 and from 0.74 to 1.50, respectively. These are intermediate between those of the gabbro-anorthosites of southwestern and southeastern Finland (*Rämö*, 1991, Table 2; see also Fig. 2). The quartz syenite 16711 of the Uljalegi intrusion has $(La/Yb)_N = 9.28$ and $(Eu/Eu^*)_N = 0.86$. Its chondrite-normalized REE-pattern is similar to those of the basic rocks (Fig. 2), but the contents of other trace elements are close to those in the granites of the major intrusive phase of the batholith.

The granites of the Salmi batholith are characterized by high contents of SiO_2, K_2O, F, Rb, Zr, Y, Nb, Zn, Sn, and REE (exept Eu) as well as high Fe/Mg and K/Na ratios, and low abundances of Al_2O_3, CaO, MgO, and Sr (Table 2; see also *Velikoslavinskiy* et al., 1978). Nb, Sn, Be, U, Th, Y, Rb, Li, and F are strongly enriched in the latest intrusive phases. Compared to the other anorthosite-rapakivi granite complexes of the East European platform the granites of the Salmi batholith are distinguished by their high SiO_2, FeO, and Fe_2O_3 contents and low TiO_2,

Table 2. *Major and trace element chemistry*

Sample	7–122	4–182	4–119	4–159	16710	16711	16709	8–210	8–165	41	2002	403–13
SiO_2	52.59	46.85	47.50	54.45	66.68	67.53	71.54	71.11	71.49	76.45	74.03	75.60
TiO_2	1.79	4.24	4.51	1.67	0.61	0.42	0.48	0.41	0.34	0.15	0.12	0.07
Al_2O_3	21.80	11.60	13.30	16.80	13.02	14.81	12.34	13.70	14.50	12.65	13.55	13.60
Fe2O3	1.52	0.38	0.78	1.14	1.34	1.02	1.14	1.49	1.05	0.71	1.40	0.38
FeO	6.14	18.56	14.15	8.78	5.33	3.11	3.22	2.43	2.18	0.85	0.90	1.79
MnO	0.08	0.26	0.23	0.14	0.09	0.06	0.06	0.07	0.06	0.04	0.02	0.03
MgO	0.82	3.40	4.13	1.44	0.33	0.23	<0.20	0.28	0.40	0.26	0.33	0.22
CaO	9.15	8.35	8.39	6.08	2.43	1.69	1.52	1.51	1.56	0.97	0.75	0.97
Na_2O	4.11	2.43	2.75	3.85	2.73	2.67	3.46	3.05	3.15	3.00	3.25	2.23
K_2O	0.89	1.05	1.10	2.77	5.44	6.64	4.39	5.21	5.78	3.50	4.71	4.45
P_2O_5	0.63	1.87	1.72	0.63	0.06	0.06	0.04	0.07	0.07	<0.03	<0.03	<0.03
F	0.05	0.11	0.14	0.05	0.06	0.04	0.09	0.30	0.14	0.21	0.38	1.10
L.O.I.	0.75	1.07	1.15	1.44	<0.50	<0.50	<0.50	1.10	0.78	0.51	0.99	1.19
H_2O-	0.09	0.18	<0.01	<0.01				0.11	0.13	<0.01	0.15	0.14
Total	100.41	100.35	99.85	99.24	98.12	98.28	98.28	100.84	101.49	99.30	100.58	101.77
$-O=F_2$	0.02	0.05	0.06	0.02	0.03	0.02	0.04	0.13	0.06	0.09	0.16	0.46
Total	100.39	100.30	99.79	99.22	98.09	98.26	98.24	100.71	101.43	99.21	100.42	101.31
Rb	8	35	25	6	174	138	132	171	140	238	377	893
Li	9		19	9				42	28	42	80	686
Sr	576	549	339	396	140	168	128	119	124	34	11	42
Y	26	37	44	59	81	47	40		51	59	143	
Zr	41	901	397	363	1044	653	375	621	453	400	255	59
Nb	19	32	36	33	73	37	20		33	84	80	
Pb	<5	12	6	16	25	25	24		26		38	
Th	<5	<5	<5	7	8	<5	<5		22	16	31	
Ba	434	4610	452	195	1973	2530	1057		1063		302	
Ni	84	7	22	10	45	27	23		15		84	
Co	10	12	29	26	<10	<10	<10		30	<10	<10	
V	46	41	153	172	14	13	11		<30		<30	
La	23.3		57.7			56.7			153	95.6		30.0
Ce	57.5		132			120			318	215		45.1
Nd	33.0		75.6			61.3			111	85.8		39.8
Sm	6.68		14.7			11.8			16.9	17.4		8.02
Eu	3.14		3.41			3.04			1.91	0.62		0.126
Gd	6.13		12.9			9.85			12.4	15.2		4.23
Dy	4.67		9.66			8.23			10.4	16.1		5.83
Er	2.34		4.95			4.46			5.66	9.45		4.77
Yb	1.91		4.31			4.12			5.06	8.91		8.13
Lu						0.635						1.20
$(Eu/Eu^*)_N$	1.50		0.74			0.86			0.40	0.12		0.07
$(La/Yb)_N$	8.24		9.05			9.28			20.4	7.25		2.49

Oxides and fluorine in wt%, trace elements in ppm; L.O.I. = loss on ignition. Trace elements determined by XRF on VRA-30 spectrometer (Carl Zeiss Jena), REE by isotope dilution at the Institute of ore deposit geology (IGEM), Moscow, the precision and accurracy is 2% or better. Samples: 7–122 - anorthosite, 4–182 - olivine gabbronorite, 4–119 - gabbronorite, 4–159 - monzonite, 8–210 - pyterlite, 8–165 - wiborgite, 41 - coarse-grained biotite granite, 2002 - fine-grained biotite porphyry granite, 403–13 - coarse-grained albite-lithian siderophyllite granite, 16709 - coarse-grained amphibole-biotite granite, 16710, 16711 - quartz syenites

Al_2O_3, MgO, CaO, and F abundances (*Velikoslavinskiy* et al., 1978; *Vorma*, 1976; *Rämö* and *Haapala*, 1991).

REE abundances in the granites of the batholith are similar to those in the Finnish rapakivi granites (cf. *Rämö*, 1991). The only distinction is that, in the Salmi

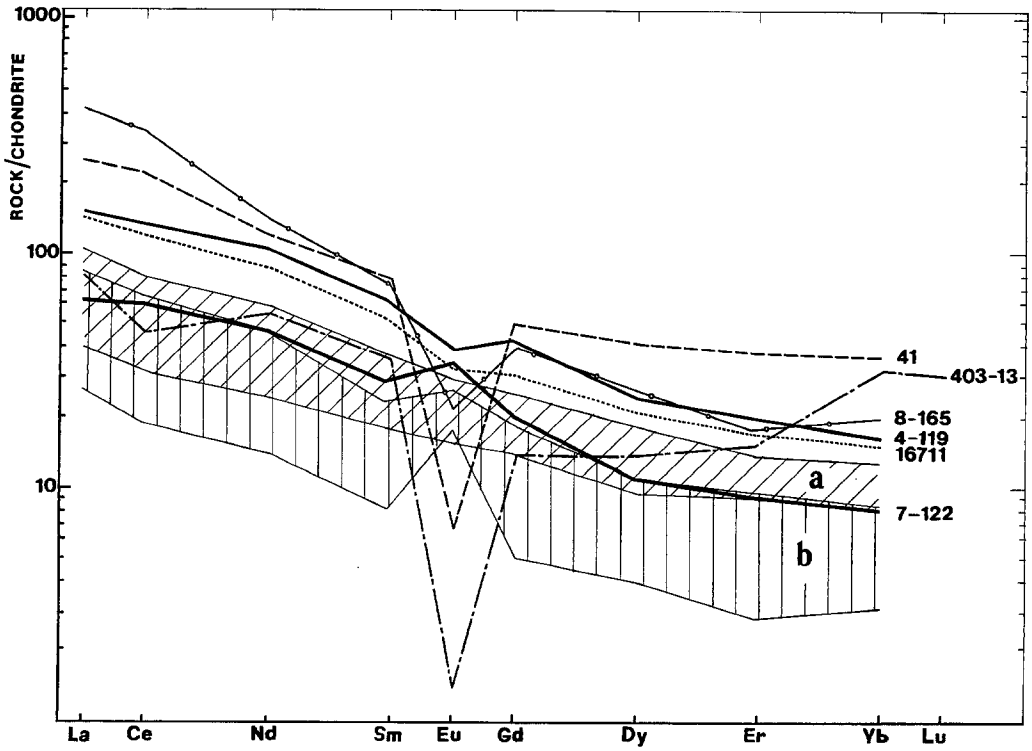

Fig. 2. Chondrite-normalized (*Taylor* and *McLennan*, 1985) REE patterns of rocks in the Salmi batholith. *7–122* anorthosite, *4–119* gabbronorite, *16711* quartz syenite, *8–165* coarse-grained amphibole-biotite granite (wiborgite), *41* even-grained biotite granite, *403–13* albite-lithian siderophyllite granite. Labeled fields denote southwestern (*a*) and southeastern (*b*) Finnish gabbroic-anorthositic rocks (*Rämö*, 1991)

batholith, the earliest amphibole-biotite granite (sample 8–165, Table 2) is most fractionated in LREE, with a $(La/Yb)_N$ ratio of 20.4 and a pronounced negative Eu anomaly ($[Eu/Eu^*]_N = 0.40$). The later intrusive phases are characterised by different REE patterns: the contents of LREE decrease and those of HREE increase, together with an increase in the negative Eu anomaly. The $(La/Yb)_N$ ratio decreases to 7.25 and $(Eu/Eu^*)_N$ becomes as low as 0.12 (sample 41, Table 2). This is possibly caused by fractionation of feldspars, clinopyroxene, and hornblende as well as accessory minerals like zircon and fluorite (concentrators of HREE) and allanite (concentrator of LREE). The albite-lithian siderophyllite granite (sample 403–13) shows a different REE distribution pattern (Fig. 2). It is relatively low in REE and its negative Eu anomaly is extreme ($[Eu/Eu^*]_N = 0.07$). The Yb content is practically unchanged as compared with the biotite granites and so the $(La/Yb)_N$ ratio is low (2.49). This may be related to stabilization of halogene complexes in a fluid-saturated melt (*Nurmi* and *Haapala*, 1986; *Kolker* et al., 1990) or to metasomatic processes producing secondary fluorite.

The tectonic setting of the Salmi batholith, the occurrence of late lithium-fluorine granites, and the geochemical specialization of the granites (high K, Rb, Nb, Y, Zr, REE except Eu, F, Sn, Be, and Li, and the REE patterns) indicate that these granites are similar to subalkaline A-type granites. According to the tectono-magmatic

classification of *Pearce* et al. (1984), they fall into the field of within plate granites (see *Amelin* et al., 1991, Fig. 12).

Geochronology

New U–Pb geochronological data on the Salmi batholith are presented in Table 3 and Fig. 3. Apatites from two anorthosites and a gabbronorite gave almost concordant U-Pb data with a mean weighted average $(^{207}Pb/^{206}Pb)_{rad}$ age of 1563 ± 9 Ma. Zircons from pyterlites of the major intrusive phase are slightly discordant and define an upper concordia intercept age of 1543 ± 8 Ma. This is compatible with the 1539 ± 11 Ma U–Pb zircon age reported by *Suominen* (1991) for the pyterlites of the batholith. These results indicate an age difference between the gabbro-anorthosites and the major rapakivi granite intrusive phase. Zircons from the fine-grained biotite granites (third intrusive phase) display more discordant U–Pb ages and give a less precise upper intercept age of 1517 ± 47 Ma.

An older inherited zircon component was revealed from air-abraded zircons separated from K-feldspar ovoids (Fig. 3). The $^{207}Pb/^{206}Pb$ ages of these zircons are up to 1.8 Ga. An interesting feature of the data is that zircons separated from K-feldspar ovoids exhibit elevated $(^{208}Pb/^{206}Pb)_{rad}$ ratios (up to 0.23) when com-

Table 3. *U-Pb isotopic data for zircons from the rapakivi granites and apatites from the basic rocks of the Salmi batholith*

Sample	Fraction weight, size	Concentrations (ppm) U	Pb	$^{206}Pb^*/^{204}Pb$	$^{206}Pb^*/^{207}Pb$	$^{206}Pb^*/^{208}Pb$	$^{206}Pb^{**}/^{238}U$	$^{207}Pb^{**}/^{235}U$	Age, Ma $^{207}Pb/^{206}Pb$
				Zircons					
8/165	3.3 mg	1118	216	970.0	9.312	5.844	0.1727	2.2288	1500±2
	7.9 mg, <0.1 mm	417	109	1793	9.742	5.317	0.2335	3.0664	1533±2
	2.3 mg, <0.1 mm, abr. 20%***	262	58.4	1146	9.349	5.076	0.1967	2.5855	1534±1
8/210	4.0 mg, <0.1 mm	432	102	1390	9.541	5.734	0.2120	2.7829	1533±4
2002	3.1 mg	372	64.3	278.8	7.040	2.882	0.1274	1.6485	1504±2
	2.2 mg, abr. 50%***	330	57.3	263.5	6.904	3.107	0.1304	1.6857	1504±4
	2.4 mg	377	70.7	300.8	7.281	3.028	0.1412	1.8029	1480±8
263/3	1.6 mg, >0.1 mm, abr. 10%***	116	36.5	927.9	7.810	4.458	0.2680	4.2115	1863±1
	1.1 mg, >0.1 mm, abr. 30%***	98.7	44.2	114.2	4.617	1.979	0.2631	3.6077	1614±3
	4.7 mg	148	39.8	331.7	7.321	3.352	0.2087	2.7687	1551±6
	4.1 mg	377	94.4	322.2	7.365	4.145	0.2011	2.6086	1510±2
	9.0 mg	181	46.7	464.7	8.071	3.977	0.2105	2.7593	1529±4
	6.9 mg	129	34.3	473.4	8.077	3.879	0.2170	2.8573	1537±4
				Apatites					
7/122	102 mg	6.36	4.89	80.6	3.785	0.706	0.2679	3.5775	1569±7
5/203	124 mg	6.15	4.62	123.7	4.857	0.633	0.2743	3.6672	1567±4
4/119	12.8 mg	5.57	5.40	56.4	2.977	0.590	0.2734	3.6428	1560±11
	29.9 mg****	5.52	5.23	58.3	3.049	0.595	0.2709	3.6027	1557±10

* Measured ratios; ** Data corrected for mass-fractionation, blank and common lead; *** Residue after air-abrasion in wt%; **** Replicate analysis

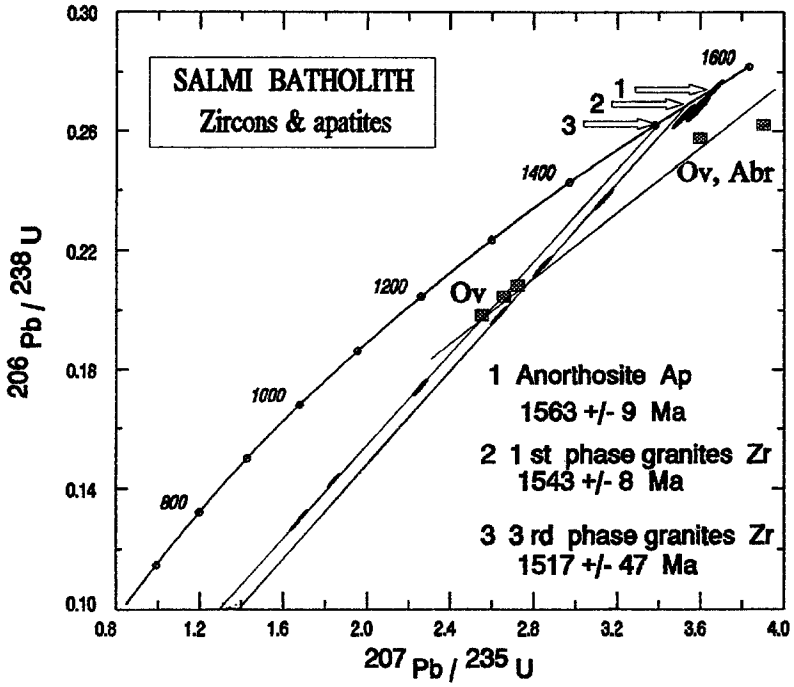

Fig. 3. Concordia diagram showing zircons and apatites from granites and gabbro-anorthosites of the Salmi batholith. *Ap* apatite, *Zr* zircon, *Ov* zircon separated from K-feldspar ovoids (sample 263/3), Abr—air-abraded zircons, 1st phase granites—coarse-grained amphibole-biotite granites (samples 8–165 and 8–210), 3rd phase granites—fine-grained biotite granite (sample 2002)

pared to zircons from bulk pyterlites (0.14 to 0.17). Particularly, this concerns zircons with elevated $^{207}Pb/^{206}Pb$ ages (Table 3). This means that the Th/U ratio in these zircons and consequently in their source or the magma from which they crystallized must have been abnormally high. One interpretation of the data is that these characteristics are inherited from an older granulite-facies lower crustal protolith of the granites and that the ovoids would represent incompletely melted residues of the protolith. For example, zircons from lower crustal granulitic xenoliths in kimberlites in the Belomorian (While Sea) region show a $(^{208}Pb/^{206}Pb)_{rad}$ ratio of 0.29 (*A. Vetrin*, pers. commun., 1992). These data imply a lower crustal origin for the rapakivi granites of the Salmi batholith. Comparable elevated $^{208}Pb/^{206}Pb$ ratios (but not corrected for initial Pb) were reported from zircons in some Finnish rapakivi granites (*Vaasjoki* et al., 1991).

Two Sm-Nd mineral errorchrons (whole rock, plagioclase, apatite, orthopyroxene, clinopyroxene, amphibole) for the basic rocks were obtained (Table 4, Fig. 4). The 1552 ± 69 Ma (MSWD = 3.3) age of the anorthosite 7/122 and the 1527 ± 130 Ma (MSWD = 2.1) age of the gabbronorite 4–119 are less precise than the U–Pb ages but are the same within the error limits. A Rb–Sr mineral errorchron (whole rock, biotite, K-feldspar, amphibole, plagioclase, apatite) was constructed for the amphibole-biotite granites 8–165 and 8–210 dated by the U–Pb method (Table 4, Fig. 5). The age of 1455 ± 17 Ma (MSWD = 4.5) is interpreted as the time of termination of post-magmatic processes within the batholith.

Table 4. *Sm–Nd and Rb–Sr analytical data and model parameters*

Sample	Rock, mineral	Sm (ppm)	Nd (ppm)	$^{147}Sm/^{144}Nd$	$^{143}Nd/^{144}Nd \pm 2\sigma_m$*	$\varepsilon_{Nd}(T)$	T_{DM}**** (Ma)	Rb (ppm)	Sr (ppm)	$^{87}Rb/^{86}Sr$	$^{87}Sr/^{86}Sr \pm 2\sigma_m$*	$^{87}Sr/^{86}Sr$ (T)
					Salmi batholith							
7-122	anorthosite	13.1	66.7	0.1179	0.511500 ± 8	− 6.5**	2599	9.68	608	0.0443	0.70621 ± 2	0.70522**
	plagioclase	0.426	4.0	0.0632	0.510896 ± 8							
	clinopyroxene	13.0	39.6	0.1977	0.512289 ± 6							
	orthopyroxene	2.78	7.9	0.2099	0.512426 ± 9							
	pyroxenes + amphibole	5.59	16.7	0.2015	0.512323 ± 7							
	apatite	36	1870	0.1172	0.511513 ± 8			0.096	328	0.0008	0.70531 ± 2	0.70529**
4–119	gabbronorite	16.0	82.9	0.1161	0.511417 ± 6	− 8.2**	2701					
	plagioclase	0.973	7.20	0.0815	0.511039 ± 6							
	clinopyroxene	15.6	54.4	0.1732	0.511975 ± 4							
	orthopyroxene	2.30	9.65	0.1438	0.511653 ± 5							
	apatite	300	1628	0.1112	0.511357 ± 5							
4–182	gabbronorite	21.1	108	0.1179	0.511446 ± 9	− 7.5**	2684	10.9	341	0.0924	0.70778 ± 3	0.70571**
8–165	wiborgite	17.6	118	0.0899	0.511195 ± 7	− 7.0***	2633	160	135	3.329	0.77987 ± 3	0.70530***
	plagioclase							96.4	180	1.494	0.73998 ± 2	
	apatite							4.12	109	0.1049	0.70964 ± 3	
	amphibole							15.3	22.9	1.868	0.74745 ± 2	
	orthoclase							307	189	4.557	0.80440 ± 2	
	biotite							726	9.24	411.8	9.65436 ± 22	
8–201	pyterlite	28.2	204	0.0840	0.511107 ± 4	− 7.6***	2678					
8–210	pyterlite	21.0	147	0.0865	0.511153 ± 6	− 7.2***	2645	200	122	4.603	0.80843 ± 10	0.70532***
	apatite							1.70	100	0.0472	0.70927 ± 2	
41	biotite granite	21.4	111	0.1166	0.511469 ± 5	− 7.0***	2627					
403–13	topaz-bearing granite	2.91	11.6	0.1513	0.511750± 4	− 8.3***	2738					
					Uljalegi intrusion							
16709	amph.-biot. granite	9.01	47.4	0.1149	0.511345 ± 5	− 8.9***	2796	132	130	2.967	0.77233 ± 4	0.70587***
16710	quartz syenite	24.5	132	0.1124	0.511416 ± 6	− 7.2***	2644	175	141	3.622	0.78608 ± 4	0.70495***
16711	quartz syenite	13.1	70.0	0.1134	0.511465 ± 16	− 6.2***	2582	141	168	2.452	0.76215 ± 3	0.70723***
					Country rocks							
700–3	schist	5.64	32.4	0.1051	0.511456 ± 6	− 4.9***	2463	259	194	3.912	0.81498 ± 3	0.72736***
265	gneiss-granite	3.01	17.7	0.1025	0.511016 ± 6	− 13.1***	3117	71.2	423	0.4870	0.71975 ± 3	0.70884***

$^{143}Nd/^{144}Nd$ ratios are normalised to La Jolla $^{143}Nd/^{144}Nd = 0.511860$. Chondritic values used to calculate $\varepsilon_{Nd}(T)$ were $^{143}Nd/^{144}Nd = 0.51264$ and $^{147}Sm/^{144}Nd = 0.1966$ (Wasserburg et al., 1981).

* Uncertainties in the last decimal places; ** Initial values calculated at 1560 Ma; *** Initial values calculated at 1540 Ma; **** Two-stage model ages after Liew and Hofmann (1988) with the first stage $^{147}Sm/^{144}Nd$ ratio of 0.1285, $^{147}Sm/^{144}Nd$ of 0.2136 and $^{143}Nd/^{144}Nd$ (0) = 0.513149 were accepted for DM (Goldstein and Jacobsen, 1988)

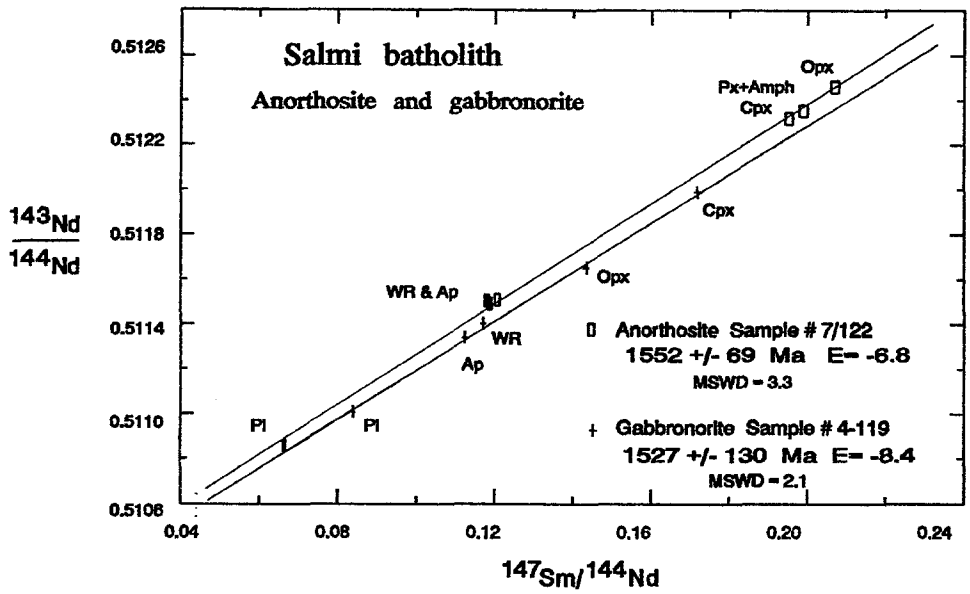

Fig. 4. Sm–Nd isochron plot for anorthosites and gabbronorites of the Salmi batholith (samples 7/122 and 4–119)

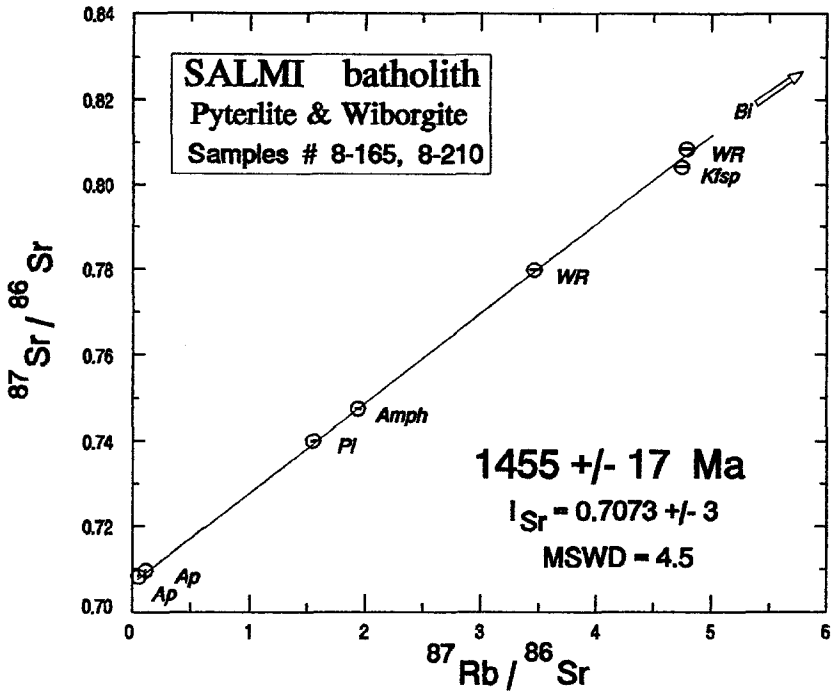

Fig. 5. Rb–Sr mineral isochron plot for the coarse-grained amphibole-biotite granites of the Salmi batholith (wiborgite 8–165 and pyterlite 8–210)

Isotope Geochemistry

Pb isotopic data obtained for both acid-leached plagioclases and K-feldspars are presented in Table 5 and Fig. 6. Plumbotectonics model growth curves after Zart-

Table 5. *Pb isotope data for acid-leached feldspars*

Sample	Mineral	$\frac{^{206}Pb}{^{204}Pb}$	$\frac{^{207}Pb}{^{204}Pb}$	$\frac{^{208}Pb}{^{204}Pb}$	μ_2	κ_2	T_{model} (Ga)
			Basic rocks				
7/122	Plagioclase	14.852	14.977	34.670	8.62	3.93	1.92
5/203	Plagioclase	14.863	14.984	34.681	8.66	3.93	1.92
4/182	Plagioclase	14.792	14.982	34.649	8.77	3.99	1.98
4/159	Plagioclase	14.796	14.994	34.692	8.86	4.04	2.00
	Plagioclase*	14.772	14.991				
	Orthoclase	14.786	14.976	34.623	8.73	3.96	1.97
4/119	Plagioclase	14.816	14.980	34.671	8.71	3.98	1.96
	Orthoclase	15.213	15.130	35.042	9.17	3.96	1.85
	Orthoclase*	15.153	15.124				
			Amphibole-biotite granites				
8–210	Plagioclase	14.936	14.983	34.810	8.53	3.99	1.85
	Orthoclase	14.808	14.975	34.766	8.69	4.10	1.96
8–165	Orthoclase	14.875	14.987	34.848	8.66	4.11	1.91
8–201	Orthoclase	14.837	14.989	34.816	8.77	4.12	1.95
G–119	Orthoclase	14.997	15.066	35.204	9.05	4.38	1.94
S–305–14	Orthoclase	15.105	15.046	35.093	8.73	4.11	1.80
	Orthoclase*	14.953	15.039				
1534	Orthoclase	15.246	15.110	35.149	8.98	4.02	1.79
			K-feldspar ovoids from amphibole-biotite granites				
S–8/4		14.887	15.000	34.864	8.74	4.12	1.92
S–8/5		14.980	15.052	35.067	8.97	4.24	1.93
			Biotite granites				
1536	Orthoclase	15.027	15.041	35.038	8.13	4.14	1.87
1537	Orthoclase	15.022	15.093	35.225	9.21	4.38	1.96
41	Plagioclase	14.959	15.048	35.036	8.98	4.23	1.94
S–329–4	Orthoclase	15.183	15.065	35.125	8.75	4.06	1.76
G-14	Orthoclase	15.081	15.047	35.120	8.77	4.17	1.82
	Orthoclase*	15.027	15.042				
S–345–9	Orthoclase	14.988	15.052	35.077	8.96	4.24	1.92
2002	Plagioclase	15.044	15.056	35.138	8.90	4.24	1.88
	Orthoclase	15.008	15.031	35.023	8.77	4.15	1.87
	Albite	15.045	15.041	35.061	8.78	4.15	1.84
			Topaz-bearing albite-lithian siderophyllite granite				
403–13	Albite	15.272	15.061	35.132	8.61	3.96	1.68

Isotopic ratios are corrected for mass-fractionation of 0.013% per amu. Model parameters were calculated according to Stacey and Kramers (1975).
* Data corrected for in situ U-decay

man and *Doe* (1981) are also shown. Main features of the data are low model μ_2 values (8.6 to 9.1) and elevated κ_2 values (3.9 to 4.4) calculated according to *Stacey* and *Kramers* (1975). Pb model ages range from 1.8 to 2.0 Ga, being considerably higher than the U–Pb ages of the batholith. The data again indicate U-depleted, old protoliths for the silicic and basic rocks of the Salmi batholith. The scatter of Pb isotopic ratios in the studied feldspars cannot be explained with variable amounts

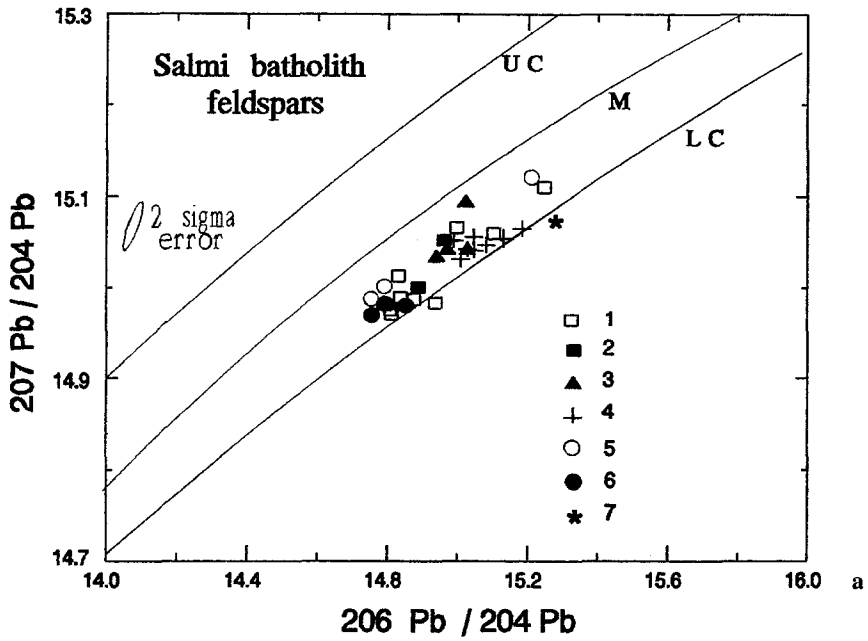

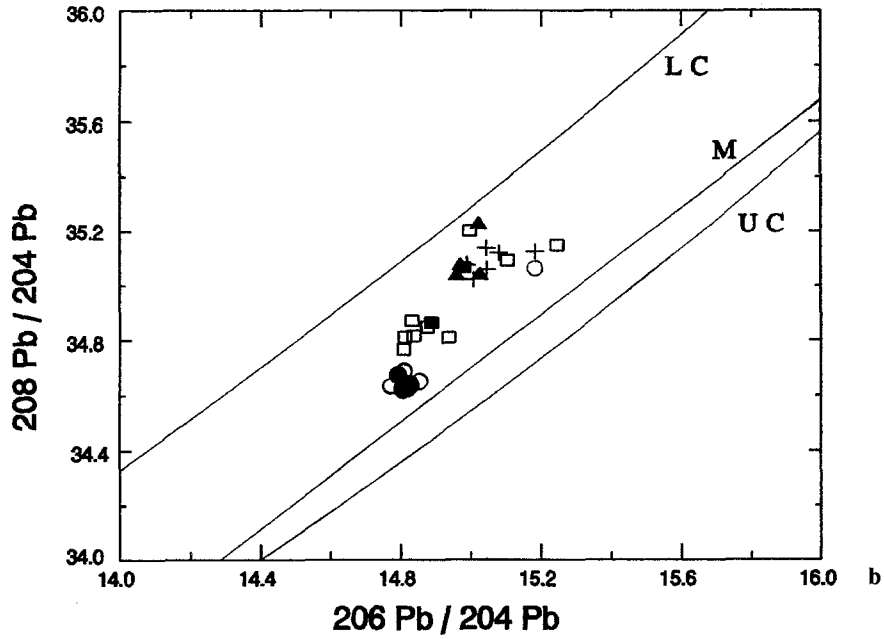

Fig. 6. $^{207}Pb/^{204}Pb$ vs. $^{206}Pb/^{204}Pb$ **(a)** and $^{208}Pb/^{206}Pb$ vs. $^{206}Pb/^{204}Pb$ **(b)** plots of feldspars (plagioclases and K-feldspars) from the amphibole-biotite granites *1*, K-feldspar ovoids *2*, even-grained biotite granite *3*, fine-grained biotite granites *4*, gabbronorites *5*, anorthosites *6*, and topaz-bearing granites *7* of the Salmi batholith. *Zartman* and *Doe* (1981) growth curves are also shown. *UC* upper crust, *M* mantle, *LC* lower crust

of radiogenic Pb because of the rather steep slope of the linear trend in the $^{207}Pb/^{204}Pb$–$^{206}Pb/^{204}Pb$ plot (Fig. 6a). Concentrations of U and Pb were measured for four selected acid-leached feldspar residues which gave a range from 0.025

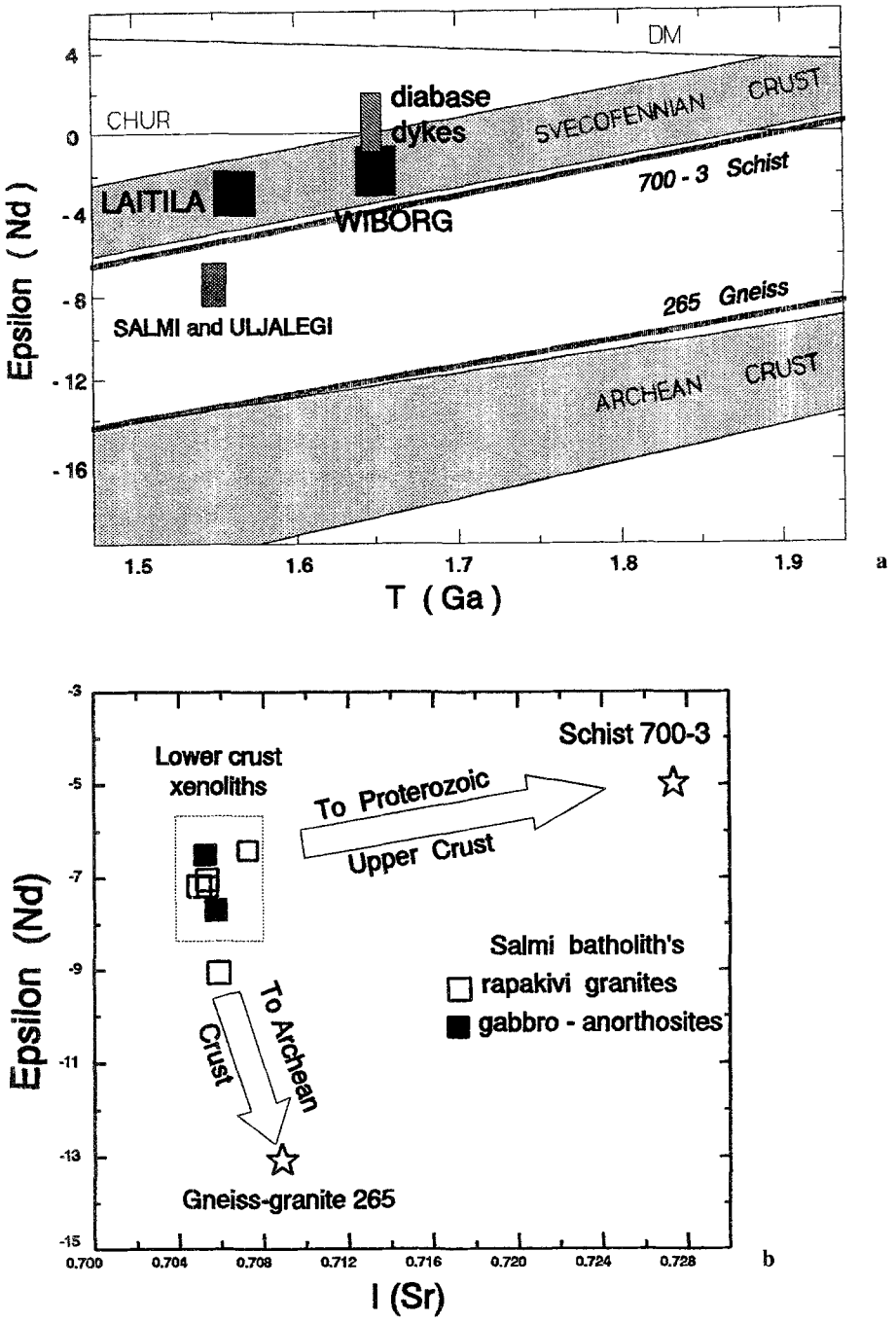

Fig. 7. **a** ε_{Nd} vs. age plot for the rapakivi granites and related rocks of the Fennoscandian shield. Data for Wiborg and Laitila areas are from *Rämö* and *Haapala* (1991). Evolution paths for the Archean and Svecofennian crust (*Huhma*, 1986; *Patchett* and *Kouvo*, 1986) and for the country rocks of the Salmi batholith are also shown. Marked in the figure are also the evolution lines of undifferentiated Earth *CHUR* and depleted mantle *DM* (*Goldstein* and *Jacobsen*, 1988). **b** ε_{Nd} (1.55 Ga) vs. I_{Sr} (1.55 Ga) plot for the rocks of the Salmi batholith. Directions of possible contamination with Archean and Proterozoic upper crust and isotopic data for lower crustal granulitic xenoliths from the eastern Fennoscandian shield (*Neymark* et al., unpublished data) are also shown

to 0.22 ppm for U and from 17.9 to 63.9 ppm for Pb. The Pb isotopic compositions corrected for in situ U-decay are given in Table 5. The correction did not measurably change the differences in the $^{207}Pb/^{204}Pb$ ratios. An increase of the K-feldspar $^{207}Pb/^{204}Pb$ ratios in the sequence ovoids—amphibole granite—biotite granite—topaz-bearing granite may point to long-term post-magmatic rock-fluid interaction under open-system conditions. It is supported by the correlation between oxygen and Pb isotope ratios (unpublished data of the authors). A remarkable feature of the Pb isotope data is that the data points of the basic rocks in the conventional Pb–Pb plot (Fig. 7a) are located in the lower part of the trend and are shifted towards the lower crustal area but not towards the mantle growth curve as modeled by *Zartman* and *Doe* (1981).

The initial ε_{Nd} values for all studied rock types vary within the range from -8.9 to -6.2 (Table 4). This suggests that a lower crustal source of late Archean age (or another old LREE-enriched source) was involved in the formation of both the basic rocks and the granites. *Rämö* and *Haapala* (1991) suggested on the basis of Sm–Nd data that the origin of the granites of the Salmi batholith involved a mixture of Proterozoic and Archean crust. This could be a plausible explanation of the Nd data alone as the Salmi data are placed between the evolution of Proterozoic and Archean crust (Fig. 7a). The evolution lines of the country rocks of the batholith (schist 700–3 and granite gneiss 265) are very close to the evolution paths of average Svecofennian and Archean crust, respectively (*Huhma*, 1986; *Patchett* and *Kouvo*, 1986; *Rämö* and *Haapala*, 1991). Our Sr isotope data provide further constraints to the model and preclude Proterozoic upper crustal material as a major component in such mixing. I_{Sr} (1.54 Ga) values for the Salmi batholith are about 0.705 and thus measurably lower than the values for the enclosing Proterozoic and late Archean rocks (Table 4).

Discussion

The problem of the genesis of the anorthosite-rapakivi granite assemblage is complicated and has not been adequately resolved yet. One of the key questions is the relation of the gabbro-anorthosites to the granites. Most authors consider lower crust as the source for the rapakivi granites and mantle for the basic rocks. *Barker* et al. (1975) suggested a model in which convecting alkali olivine basalt magma produces the gabbro-anorthosite complexes. Interaction of this magma with the lower crust forms a secondary quartz syenite magma that produces the mangerite-syenite complexes. Interaction of this secondary melt with the middle crust results in a more silicic magma from which the potassium-rich biotite and amphibole-biotite granites (rapakivi granites) crystallize. According to *Bridgwater* and *Windley* (1973) the gabbro-anorthosites are produced from mantle-derived basaltic magma and the rapakivi granites from a magma generated by the influence of a mantle diapir on the material of the lower crust. Some authors (*Velikoslavinskiy* et al., 1978; *Higgins* and *Doig*, 1981) suggest the upper mantle to be the source for the whole assemblage. Further, there are concepts that the parental magma was generated as a result of mixing of a mantle-derived basaltic magma and a secondary anatectic magma formed by partial melting of lower crustal material (e.g., *Kranck*, 1969).

The gabbro-anorthosites and rapakivi granites of the Salmi batholith are practically coeval and have alike initial Nd, Sr, and Pb isotope compositions. This does not

contradict with the assumption of a single source for these rocks and could prove their comagmatic character. A single source was also considered for the Finnish rapakivi granites and associated basic rocks by *Patchett* et al. (1981) as they demonstrated similar ε_{Hf} values for the granites and the basic rocks. In the light of more representative Nd isotopic data *Rämö* (1991) explained this similarity with unrepresentative sampling. For the Salmi batholith, the same conclusion could be made, as only three Nd isotopic samples are available from the basic rocks and as, in the conventional Pb–Pb plot (Fig. 6a), feldspars from the basic rocks and granites (at least from amphibole-biotite granites) overlap. Yet then, the basic rocks and the granites appear to have different $^{208}Pb/^{204}Pb$ ratios and κ_2 values (Table 5; Fig. 6b). These differences are not likely to be due to incomplete leaching of radiogenic ^{208}Pb and may indicate different sources for the basic rocks and the granites.

The positive to slightly negative ε_{Nd} values of the Finnish diabase dykes and gabbro-anorthosites (*Rämö*, 1991) require that they were derived from sources with a chondritic or LREE-depleted character. In this regard, the basic rocks of the Salmi batholith with their much more negative ε_{Nd} values are anomalous. This can be attributed either to contamination of the parental magmas of the gabbro-anorthosites with ancient silicic crust or to derivation of the parental magmas from "enriched mantle". Anorthosites and mafic intrusions in Labrador (Kiglapait, Flowers River, Harp Lake, and Shabogamo) also have negative ε_{Nd} values (*Ashwal* and *Wooden*, 1985). *Zindler* et al. (1981) suggested that the ε_{Nd} of -5.3 in the Shabogamo gabbro may have been caused by 20% assimilation of a granitic component derived from late Archean (2.7 Ga) silicic crust.

It is possible to estimate the contribution of Archean crust to the basic rocks of the Salmi batholith by using a two-component mixing equation (*Faure*, 1986). Mixing x parts of Archean and one part of mantle-derived material to yield the isotopic composition of the basic rocks of the Salmi batholith is described by the equation

$$x = \frac{C_{Nd}(M)(\varepsilon_{Nd}(Sal) - \varepsilon_{Nd}(M))}{C_{Nd}(Arch)(\varepsilon_{Nd}(Arch) - \varepsilon_{Nd}(Sal))}$$

where $C_{Nd}(i)$ is the concentration of Nd in component i, $\varepsilon_{Nd}(i)$ is the ε_{Nd} value of component i, M and Arch denote mantle and Archean components, respectively, and Sal the Salmi batholith. Accepting for the mantle component the values of the less contaminated Finnish diabase dykes ($C_{Nd} = 35$ ppm, $\varepsilon_{Nd} = +1$; *Rämö*, 1991) and for the Archean component those of the granite gneiss 265 ($C_{Nd} = 18$ ppm, $\varepsilon_{Nd} = -13$), a value of 70% is calculated for the Archean crustal component in the basic rocks of the Salmi batholith with $\varepsilon_{Nd} = -6.5$ (highest measured value). Larger amounts of contamination would be required if the original gabbro-anorthosite magma had a Nd isotopic signature of more depleted mantle. A crustal contaminant with ε_{Nd} value of -20 and $C_{Nd} = 20$ ppm would contribute about 50% of the material. Such could be the Archean tonalitic gneisses of the Vodlozero block 200 km east of the Salmi batholith which have an U–Pb zircon age of about 3.2 Ga and neodymium T_{DM} model age of 3.6 Ga (*Lobach-Zhuchenko* et al., 1992). The gneisses show, however, elevated feldspar $^{207}Pb/^{204}Pb$ ratios (*Ovchinnikova* et al., 1990) which precludes them as a plausible contaminant. Contamination with the rapakivi granite parental magma ($C_{Nd} = 100$ ppm, $\varepsilon_{Nd} = -7.5$) gives a figure of 70% for the granitic component. All these estimates seem unreasonable in the light of major

element constraints. For example, the SiO_2 content in the gabbronorite 4–119 which shows an ε_{Nd} value of -8.2 is only 47.5%.

Bulk contamination with crustal materials thus cannot explain the isotopic and chemical composition of the basic rocks of the Salmi batholith. Selective incorporation of LREE and other incompatible elements into the basic magma is needed to explain the data. Alternatively, the gabbro-anorthosites could have been derived from mantle sources with long-term enrichment in LREE. The implication of this would be that the gabbro-anorthosites of southeastern Fennoscandia tapped isotopically distinct mantle sources. It is possible that the Raahe-Ladoga zone of the Fennoscandian shield (roughly coinciding with the Karelian Province in Fig. 1) represents the surface expression of a deep boundary which separates lithospheres of different affinity.

Recent results by *Rämö* (1991) on the Nd and Pb isotopes of the Finnish rapakivi granites and related basic rocks have clearly shown that these rocks assemblages were not comagmatic. We also suggest different sources for the gabbro-anorthosites and granites of the Salmi batholith. In this case the sources must have had almost identical isotopic features. *Rämö* and *Haapala* (1991) and *Rämö* (1991) suggested that the granites of the Salmi batholith are probably about one-to-one mixtures of Proterozoic and Archean lower crustal materials. An alternative to the two-component mixing origin is that the granites were derived from a single crustal source with two-stage neodymium T_{DM} model ages of 2.6 to 2.7 Ga. *Rämö* (1991) argued that there is no evidence for such a source in the Fennoscandian shield. Recent results on lower crustal granulitic xenoliths from kimberlites in the eastern part of the shield (White Sea region) show a range of ε_{Nd} (1.55 Ga) values from -5.5 to -8.4, neodymium T_{DM} model ages of 2.5 to 2.8 Ga and I_{Sr} (1.55 Ga) values from 0.704 to 0.708 (unpublished data by the authors) which are very close to those observed in the granites of the Salmi batholith (Fig. 7b). The data may solve the contradiction regarding the origin of the batholith. Most studies on the genesis of the Proterozoic rapakivi granites (e.g., *Anderson*, 1983; *Rämö*, 1991) have suggested that a newly-formed juvenile crustal source is a characteristic environment for these granites. The xenoliths may represent Proterozoic basaltic underplates that formed at the boundary between lower continental crust and mantle during the Svecofennian orogeny 300 to 400 Ma before the emplacement of the Salmi batholith. Intensive interaction of mantle-derived magmas with an old Archean lower crust may have lead to formation of Proterozoic lower crust with mixed isotopic features. Nd, Pb, and Sr isotopic compositions of many mafic granulite xenoliths point to their origin by mixing of a mantle-derived magma and compositionally evolved lower crust (*Rudnick* et al., 1986; *Kempton* et al., 1990; *Rudnick* and *Goldstein*, 1990). The mafic residues of these differentiation and melting processes may return to the mantle carrying with them material that was once part of the lower continental crust (*Arndt* and *Goldstein*, 1989). Such isotopically anomalous mantle and lower crust may have been the sources for the basic rocks and granites of the Salmi batholith.

The data imply that mantle-derived magmatism was responsible for the formation of the gabbro-anorthosites. The ascent of a mantle diapir resulted in protrusion of considerable masses of basic magma at the base of the crust causing partial melting of the lower crust. The inherited zircon component in K-feldspar ovoids are also in favor of such a suggestion. Contamination of the melts with Archean and

Proterozoic upper crustal materials may have caused the scatter of the Pb, Sr, and Nd isotopic ratios (Figs. 6 and 7).

Conclusions

The new geochronological data suggest that the Salmi batholith is the youngest among the anorthosite-rapakivi granite assemblages in the Fennoscandian shield, with the main intrusive activity having occurred at about 1540 Ma. The earliest magmatism related to the intrusion of the rapakivi granites was the emplacement of anorthosites at about 1560 Ma, while tha major intrusion of rapakivi granites took place at 1543 Ma. The time gap between the crystallization of the main intrusive phases of the Salmi batholith and the completion of postmagmatic processes accompained by closing of the Rb–Sr isotope system was about 100 Ma.

The rapakivi granites of the Salmi batholith show several geochemical characteristics typical of subalkaline A-type granites and within plate granites. The initial Nd, Sr, and Pb isotopic compositions of the anorthosites and rapakivi granites of the Salmi batholith are alike in both assemblages and point to sources with low time-integrated U/Pb and Sm/Nd, intermediate Rb/Sr, and elevated Th/U ratios. Bulk contamination with crustal materials cannot explain the data for the basic rocks. Selective incorporation of LREE and other incompatible elements into basic magma is needed, or else, it was derived from an isotopically anomalous subcontinental mantle source. The ascent of a mantle diapir resulted in anatexis of the lower crust and formation of the parental magma for the rapakivi granites.

Acknowledgements

This work was supported by the advanced study funding of the Russian Academy of Sciences. Our thanks are due to Drs. *S. Yakovleva*, *G. Ovchinnikova*, and *B. Gorokhovskiy* for their assistance in obtaining U–Pb and Pb–Pb data and to Prof. *D. Velikoslavinskiy* for providing some samples and for the fruitful discussion. Some fragments of a text from a field excursion guide (*Amelin* et al., 1991) were used during the preparation of this paper. We are grateful to Mr. *B. Saltikoff* who translated the guidebook from Russian to English and to Prof. *I. Haapala*, Dr. *O.T. Rämö*, and Mr. *P. Salonsaari* who edited it. We also thank Dr. *H. Huhma* and an unknown reviewer for their comments and constructive suggestions.

References

Amelin Yu, Beljaev A, Larin A, Neymark L, Stepanov K (1991) Salmi batholith and Pitkäranta ore field in Soviet Karelia. In: *Haapala I, Rämö OT, Salonsaari PT* (eds). Geol Surv Finland Guide 33: 57

Anderson JL (1983) Proterozoic anorogenic granite plutonism of North America. In: *Medaris LG Jr, Byers CW, Mickelson DM, Shanks WC* (eds) Proterozoic geology: selected papers from an international Proterozoic symposium. Geol Soc Am Mem 161: 133–154

Arndt NT, Goldstein SL (1989) An open boundary between lower continental crust and mantle: its role in crust formation and crustal recycling. Tectonophysics 161: 201–212

Ashwal LD, Wooden SL (1985) Sm–Nd isotopic studies of Proterozoic anorthosites: systematics and implications. In: *Tobi AC, Touret JLR* (eds) The deep Proterozoic crust in the North Atlantic Provinces, pp 61–73

Barker F, Wones DR, Sharp WN, Desborough GA (1975) The Pikes Peak batholith, Colorado

Front Range, and a model for the origin of the gabbro-anorthosite-syenite-potassic granite suite. Precambrian Res 2: 97–160

Bridgwater D, Windley BF (1973) Anorthosites, post-orogenic granites, acid volcanic rocks and crustal development in the North Atlantic Shield during the mid-Proterozoic. Geol Soc South Africa Spec Publ 3: 307–317

Emslie RF (1985) Proterozoic anorthosite massifs. In: *Tobi AC, Touret JLR* (eds) The deep Proterozoic crust in the North Atlantic Provinces, pp 39–60

Faure G (1986) Principles of isotope geology, 2nd ed. Wiley, New York, 589 pp

Goldstein SJ, Jacobsen SB (1988) Nd and Sr isotopic systematics of river water suspended material: implications for crustal evolution. Earth Planet Sci Lett 87: 249–265

Higgins MD, Doig R (1981) The Sept Iles anorthosite complex: field relationships, geochronology and petrology. Can J Earth Sci 18: 561–573

Huhma H (1986) Sm–Nd, U–Pb and Pb–Pb isotopic evidence for the origin of the Early Proterozoic Svecokarelian crust in Finland. Geol Surv Finland Bull 337:48

Kempton PD, Harmon RS, Hawkesworth CJ, Moorbath S (1990) Petrology and geochemistry of lower crustal granulites from Geronimo Volcanic Field, southeastern Arizona. Geochim Cosmochim Acta 54: 3401–3426

Kolker A, Lindsley DH, Hanson GN (1990) Geochemical evolution of the Maloin Ranch pluton, Laramie anorthosite complex, Wyoming: trace elements and petrogenetic models. Am Mineral 75: 572–588

Kranck EH (1969) Anorthosites and rapakivi magmas from the lower crust. In: *Isachsen YW* (ed) Origin of anorthosites and related rocks. NY State Mus Sci Serv Mem 18: 93–97

Krogh TE (1973) A low-contamination method for hydrothermal decomposition of zircon and extraction U and Pb for isotopic age determinations. Geochim Cosmochim Acta 37: 485–494

Krogh TE (1982) Improved accuracy of U-Pb zircon ages by the creation of more concordant systems using air abrasion technique. Geochim Cosmochim Acta 46: 637–649

Liew TC, Hofmann AW (1988) Precambrian crustal components, plutonic associations, plate environment of the Hercynian Fold Belt of central Europe: indications from Nd and Sr isotopic study. Contrib Mineral Petrol 98: 129–138

Lobach-Zhuchenko SB, Chekulajev VP, Sergeev SA, Levchenkov OA, Krylov IN (1992) The oldest rocks of the Karelian granite-greenstone terraine. Precambrian Res (in press)

Ludwig KR (1987) PBDAT for MS-DOS. A computer program for IBM-PC compatibles for processing raw Pb-U-Th isotope data. US Geol Surv Open-File Rep 88–542, 40 pp

Ludwig KR (1988) ISOPLOT—a plotting and regression program for radiogenic-isotope data, for IBM-PC compatible computers, version 2. US Geol Surv Open-File Rep 88-557: 62

Manhes G, Minster IF, Allègre CJ (1978) Comparative uranium-thorium-lead and rubidium-strontium study of the Saint Severin amphoterite: consequences foe early solar system chronology. Earth Planet Sci Lett 39: 14–24

Nurmi PA, Haapala I (1986) The Proterozoic granitoids of Finland: granite types, metallogeny and relation to crustal evolution. Bull Geol Soc Finland 58: 203–233

Ovchinnikova GV, Lobac-Zhuchenko SB, Neymark LA, Krylov IN (1990) The petrology of the late-kinematic granites in South-East Karelia. Geol Zborn Geol Carp 41: 681–692

Patchett PJ, Kouvo O, Hedge CE, Tatsumoto M (1981) Evolution of continental crust and mantle heterogeneity: evidence from Hf isotopes. Contrib Mineral Petrol 78: 279–297

Patchett PJ, Kouvo O (1986) Origin of continental crust of 1.9–1.7 Ga age: Nd isotopes and U-Pb zircon ages in the Svecokarelian terrain of South Finland. Contrib Mineral Petrol 92: 1–12

Pearce JA, Harris NBW, Tindle AG (1984) Trace element discrimination diagrams for the tectonic interpretation of granitic rocks. J Petrol 25: 956–983

Rämö OT (1991) Petrogenesis of the Proterozoic rapakivi granites and related basic rocks of southeastern Fennoscandia: Nd and Pb isotopic and general geochemical constraints. Geol Surv Finland Bull 355, 161 pp

Rämö OT, Haapala I (1991) The rapakivi granites of eastern Fennoscandia: a review with insights into their origin in the light of new Sm-Nd isotopic data. In: *Gower CF, Rivers T, Ryan B* (eds) Mid-Proterozoic Laurentia-Baltica. Geol Ass Can Spec Paper 38: 401–415

Richard P, Shimizu N, Allègre CJ (1976) $^{143}Nd/^{146}Nd$, a natural tracer: an application to oceanic basalts. Earth Planet Sci Lett 31: 269–273

Rudnick RL, McDonough WF, McCulloch WF, Taylor SR (1986) Lower crustal xenoliths from Queensland, Australia: evidence for deep crustal assimilation and fractionation of continental basalts. Geochim Cosmochim Acta 50: 1099–1115

Rudnick RL, Goldstein SL(1990) The Pb isotopic composition of lower crustal xenoliths and the evolution of lower crustal Pb. Earth Planet Sci Lett 98: 192–207

Scherbak NP et al. (1989) Geochronological scale of precambrian of the Ukrainian shield. Kiev, 144 pp (in Russian)

Stacey JS, Kramers JD (1975) Approximation of terrestrial lead isotope evolution by a two-stage model. Earth Planet Sci Lett 26: 207–221

Steiger RN, Jäger E (1977) Convention on the use of decay constants in geo- and cosmochronology. Earth Planet Sci Lett 26: 359–362

Suominen V (1991) The chronostratigraphy of SW Finland with special reference to the Postjotnian and Subjotnian diabases. Geol Surv Finland Bull 356, 100 pp

Taylor SR, McLennan SM (1985) The continental crust: its composition and evolution. Blackwell Scientific Publications, Oxford London Edinburgh Boston Palo Alto Melbourne, 312 pp

Vaasjoki M (1977) Rapakivi granites and other postorogenic rocks in Finland. Their age and the lead isotopic composition of certain associated galena mineralizations. Geol Surv Finland Bull 294, 64 pp

Vaasjoki M, Rämö OT, Sakko M (1991) New U-Pb ages from the Wiborg rapakivi area: constraints on the temporal evolution of the rapakivi granite—anorthosite—diabase dyke association of southeastern Finland. In: *Haapala I, Condie KC* (eds) Precambrian granitoids—petrogenesis, geochemistry and metallogeny. Precambrian Res 51: 227–243

Velikoslavinskiy DA, Birkis AP, Bogatikov OA, Bukharev VP, Velikoslavinskiy SD, Gordienko LI, Zinozhenko OV, Kivisilla JJ, Kirs JE, Kononov YV, Levitskiy YF, Niin MI, Puura VA, Khvorov MI, Shustova LE (1978) Anorthosite-rapakivi suite. Nauka, Leningrad, 296 pp (in Russian)

Vorma A (1976) On the petrochemistry of rapakivi granites with special reference to the Laitila massif, southwestern Finland. Geol Surv Finland Bull 285, 98 pp

Wasserburg GJ, Jacobsen SB, DePaolo DJ, McCulloch MT, Wen T(1981) Precise determination of Sm/Nd ratios, Sm and Nd isotopic abundances in standard solutions. Geochim Cosmochim Acta 45: 2311–2323

Windley BF (1983) A tectonic review of the Proterozoic. In: *Medaris LG Jr, Byers CW, Mickelson DM, Shanks WC* (eds) Proterozoic geology: selected papers from an international Proterozoic symposium. Geol Soc Am Mem 161: 1–10

Zartman RE, Doe BR (1981) Plumbotectonics—the model. Tectonophysics 75: 135–162

Zindler A, Hart SR, Brooks C (1981) The Shabogamo Intrusive suite, Labrador: Sr and Nd isotopic evidence for contaminated mafic magmas in the Proterozoic. Earth Planet Sci Lett 54: 217–235

Authors' address: *L. A. Neymark, Yu. V. Amelin,* and *A.M. Larin,* Institute of Precambrian Geology and Geochronology, Russian Academy of Science, St. Petersburg 199034, Russia.